Applied Catalysis B: Environmental 236 (2018) 420–427

Contents lists available at ScienceDirect

Applied Catalysis B: Environmental

journal homepage: www.elsevier.com/locate/apcatb

Selective CO methanation with structured RuO_2/Al_2O_3 catalysts

A. Muñoz-Murillo, L.M. Martínez T.*, M.I. Domínguez, J.A. Odriozola, M.A. Centeno

Instituto de Ciencia de Materiales de Sevilla – Departamento de Química Inorgánica, Centro Mixto CSIC – Universidad de Sevilla, Avda, Américo Vespucio 49, 41092, Sevilla, Spain

ARTICLE INFO

Keywords:
RuO_2/Al_2O_3
Fecralloy micromonolith
CO and CO_2 methanation

ABSTRACT

Active and selective structured RuO_2/Al_2O_3 catalysts for CO methanation using a flow simulating CO_2-rich reformate gases from WGS and PROX units (H_2 excess, CO_2 presence and 300 ppm CO concentration) were prepared. Both, the RuO_2/Al_2O_3 powder and the slurry prepared from it for its structuration by washcoating of the metallic micromonolithic structure, were also active and selective. Both the slurry (S-RuAl) and micromonoliths (M-RuAl) were able to completely and selectively methanate CO at much lower temperatures than the parent RuAl powder. The optimal working temperature in which the CO conversion is maximum and the CO_2 conversion is minimized was determined to be from 149 °C to 239 °C for S-RuAl and from 165 °C to 232 °C for M-RuAl, whilst it was from 217 °C to 226 °C for RuAl powder. TPR, XRD and TEM measurements confirmed that the changes in the activity and selectivity for CO methanation among the considered catalysts can be related with modifications in the surface particle size of ruthenium and its reducibility. These were ascribed to the metallic substrate, the presence of PVA and colloidal alumina in the slurry preparation, the aqueous and acidic media and the thermal treatment used, resulting in a more active and selective catalysts than the parent powder.

1. Introduction

H_2 produced from the reformer stream carries significant amounts of H_2O, CO and CO_2. The decreasing (or elimination) of CO is mandatory if this hydrogen is used for feeding PEM fuel cells [1], since electrocatalysts as Pt and Pt-Ru are poisoned by irreversible adsorption of CO, said output must be purified to levels of CO below 20 ppm prior to admission to fuel cells. Nowadays there are different strategies to achieve the desired CO concentration levels. The typical solution consists in the use of different catalytic units after the reformate reactor. The first unit can be a water gas shift (WGS) reactor to transform CO into CO_2 Eq. (1)

$$CO + H_2O \leftrightarrow CO_2 + H_2;\ \Delta H^\circ = -41.2\ kJ/mol \quad (1)$$

WGS is a reaction limited by the equilibrium, kinetically favored at high temperature and is generally carried out in a series of adiabatic converters; typically two reactors, a high-temperature shift (HTS) to take advantage kinetically and a low-temperature one (LTS) to achieve higher CO conversion. Both reactors are working with well-established catalysts based on Fe-Cr and Cu-Zn, respectively [2]. However, when envisaged applying this reaction in one step or in mobile application for H_2 purification the noble metal based catalysts gain importance [3]. In any case, even with this configuration and the best catalysts used, the minimum level of CO achieved is only ~0.5%. In order to decrease the CO level until the ideal concentration before fuel cells, it is necessary to add other units. In that sense, preferential oxidation (PROX) Eq. (2) and CO methanation Eq. (3) reactors can be used as solutions.

$$CO + O_2 \rightarrow CO_2;\ \Delta H^\circ = -283\ KJ/mol \quad (2)$$

$$CO + 3H_2 \rightarrow CH_4 + H_2O;\ \Delta H^\circ = -206\ kJ/mol \quad (3)$$

The catalytic hydrogenation of carbon monoxide to methane and other hydrocarbons is currently receiving a great deal of attention [4–7]. This reaction has been widely used in industry as an efficient method for the removal of carbon oxides from H_2-rich feed gases for fuel cells or ammonia plants [8–10] since it could be used as the final purification step to reduce concentration of CO to extremely low levels. This reaction offers certain advantages, compared to preferential oxidation (PROX) because it does not require addition of oxygen (air) in the hydrogen-rich gas stream, which may give rise to various problems related to reduced hydrogen yield, dilution, safety and restrictions in the operating parameters. In addition, methane produced is inert to the PEM fuel cell electrodes and can be utilized in the afterburner. However, CO methanation consumes a large amount of valuable hydrogen (three moles per mol of CO abated) and may run in parallel with the undesired methanation of CO_2 Eq. (4), which also consume significant quantities of hydrogen, as well as with the reverse water–gas shift (RWGS) Eq. (1), which shifts CO_2 to CO. For that reason, methanation

* Corresponding author.
E-mail addresses: leidy@icmse.csic.es (L.M. Martínez T.), centeno@icmse.csic.es (M.A. Centeno).

https://doi.org/10.1016/j.apcatb.2018.05.020
Received 26 February 2018; Received in revised form 30 April 2018; Accepted 7 May 2018
Available online 12 May 2018
0926-3373/ © 2018 Elsevier B.V. All rights reserved.

reaction must be highly selective towards CO methanation, with CO_2 methanation essentially being inhibited; otherwise the loss of H_2 would become intolerable. Consequently, it is important to develop stable and selective CO methanation catalysts with sufficiently high activity at relatively low temperatures, able to suppress both CO_2 methanation and RWGS reactions. In a similar way, the use of CO methanation as an H_2 clean-up process is only economically viable if is applied as final step, when the CO concentration to be abated is in the 300 ppm level.

$$CO_2 + 4H_2 \rightarrow CO + H_2O;\ \Delta H^{\circ} = -165\ kJ/mol \quad (4)$$

Hydrogenation of carbon oxides toward methane and higher hydrocarbons can be catalyzed by several metal catalysts, including Ni [11–15], Ru [16–21] and Rh [20,22] among others. Ru is believed to be the most active methanation catalysts. When it is dispersed on metal oxide carriers have been found to exhibit high activity for the solo-methanation of CO [10,18] or CO_2 [15,23–27] as well as for the CO-methanation of CO/CO_2 mixtures [18,20,25,28]. It has been reported [29] that the specific activity of Ru/Al_2O_3 for CO hydrogenation is about one order of magnitude higher, compared to that of Al_2O_3- supported Rh or Pd. Ruthenium (and also Rh and Ni) is also very active for hydrogenation of CO/CO_2 mixtures in contrast to Pd or Pt, which tends to catalyze the RWGS reaction [12]. The activity and selectivity of Ru catalysts to CH_4 is however largely dependent on the dispersion of metallic phase, on the type of the support and addition of modifiers/promoters that can chemically interact with the metal [22]. Ru catalysts have been supported on a number of oxide materials such as Al_2O_3, TiO_2, SiO_2, MgO, $MgA_{l2}O_4$, CeO_2 [30]. The nature of the support affects the mechanism for hydrogenation reactions of CO/CO_2, since the metal support interaction modifies the adsorption of the intermediates as well as desorption of the products. In addition, catalytic performance of dispersed metal catalysts for methanation reactions is often affected by metal loading and crystallite size in a manner which depends on operating conditions used and metal–support combination employed [19].

The use of micromonoliths in methanation reaction is presented as alternative to the powder catalysts since heat and mass transport properties are strongly enhanced offering high precision in catalysis at all relevant scales of the catalytic processes. Moreover the micromonoliths present low energy input, high catalytic performance per mass unit of active phase, safer operating conditions, lower pressure drop and easiest catalysts separation, making them the structure of choice for catalytic reaction [31]. Metallic micromonoliths offer a better mechanical strength and higher thermal conductance than ceramic ones, which can be also advantageous. However, the adhesion of the catalytic layer to the metallic substrate is an important limitation. A suitable pretreatment of the micromonolith surface and the carefully control of the parameters of the catalysts deposition are mandatory [32]. Among the metallic substrates used in the literature for preparing micromonoliths, ferritic stainless steel (for instance fecralloy) is one of the most interesting due to adequate chemical and thermal stability at the temperature normally used in catalytic reactions and chemical compatibility with the catalytic layer.

In the present study, the catalytic performances of powder and micromonolithic Ru/Al_2O_3 catalysts were investigated in selective methanation reaction of CO (S-MET), using a methanation flow simulating CO_2-rich reformate gases from WGS and PROX units (H_2 excess, CO_2 presence and 300 ppm CO concentration).

2. Experimental

2.1. Micromonolith manufacture

Commercial Fecralloy stainless steel sheets 50 μm thick (Goodfellow, typical analysis Cr 22%, Al 4.8%, Si 0.3%, Y 0.3%, C 0.03%, Fe balance) were used as raw material. The foils were washed with water and soap, rinsed with acetone under sonication (30 min) and finally dried at room temperature. The micromonoliths were prepared by rolling together around an axis a flat and a corrugate sheet leading to a cylindrical-shaped body (L = 3 cm, Ø = 1.6 cm, 540 cm^2 total surface area) resulting in parallel longitudinal channels (2063 cells per square inch). The micromonoliths were thermally pretreated in an oven at 900 °C during 22 h in.order to grow a rough, homogeneous and well adhered oxide scale layer, mainly composed by α-Al_2O_3, on the metallic surface. This layer easies the catalyst anchoring on the surface, by improving the physical adhesion and the chemical compatibility [33,34].

2.2. Catalysts preparation

2.2.1. Powder catalyst

Wet impregnation was selected as synthesis method. A commercial γ- Al_2O_3 support (Sasol, Puralox Scca 30/100) was impregnated with the adequate amount of Ruthenium (III) nitrosyl nitrate solution (Johnson Matthey) diluted in water (200 ml per gram of support) in order to obtain a Ru loading of 10 wt. %. After 15 min of stirring at room temperature the solvent was removed on rotavapor and the obtained solid was dried at 130 °C for 24 h and finally calcined at 400 °C for 2 h with a heating ramp of 10 °C min^{-1}.

2.2.2. Micromonolithic catalysts

Washcoating was the selected method for the catalysts deposition on the micromonoliths. The pretreated micromonolithic structures were immersed in a slurry of RuO_2/Al_2O_3 catalyst with the adequate composition and rheological properties. The rheological properties of the slurry were properly adjusted in order to ensure a layered homogeneous deposition and to avoid cracking effects of the layer. First, the RuO_2/Al_2O_3 catalyst was milled in a zirconia jar on a Retsch® PM100 equipment until obtaining a 5 μm < ø < 10 μm particle size. Then, the adequate amount of solid was dispersed in deionised water and the mixture was sonicated using an ultrasonic disperser (Sonicator Misonix) working at 50 W. After that PVA (polyvinyl alcohol), previously dissolved in hot water, was added as tensioactive and colloidal alumina (Nyacol Al20) was also added to improve the stability. The mixture was kept under vigorous stirring for 24 h. The optimized composition of the suspension was 18.2 wt. % catalyst, 11 wt. % PVA, 6.28 wt. % colloidal alumina and distilled water as balance. The viscosity of the final slurry was 7.5 cps and the pH was 6.18. This pH value assures the stability of the slurry, avoiding catalyst particle agglomeration since the measured isoelectric point of the RuO_2/Al_2O_3 solid was 9.5.

The coating procedure consists in the immersion of the micromonolith in the prepared slurry for 1 min and then withdrawn at a constant speed of 3 cm/min. To avoid obstruction of the micromonolith channels, the excess of colloid was removed by centrifugation at 600 rpm for 10 min. Then, the micromonolith was dried at 130 °C for 30 min. The deposition process was repeated three times until 150–160 mg of catalyst was supported. Finally, the structured catalyst was calcined at the same temperature than the bare powder catalyst (400 °C, 2 h) but employing 2 °C/min heating rate. Two micromonithic catalysts were prepared in order to verify the reproducibility of the results. The weight gain was additive in both micromonoliths, increasing about 53-56 mg after each washcoating procedure (Fig. 1). After calcination, the final weight gain was 138.3 and 147.3 mg. Taking into account the amount of colloidal Nyacol used as additive (6.1 wt. %), and its relative content of alumina (20 wt.%), the real amount of the bare RuO_2/Al_2O_3 catalysts deposited was 129.6 and 138 mg, respectively. For comparative purposes, fresh prepared slurry was dried and calcined in the same way, obtaining a powder representative of the washcoated catalysts (slurried catalyst).

The bare calcined powder catalyst, the calcined slurried catalyst and the micromonolithic systems were denoted as RuAl, S-RuAl and M-RuAl respectively.

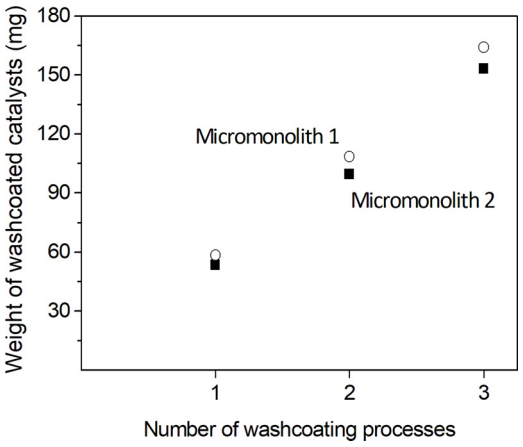

Fig. 1. Weight gain comparison between two micromonoliths before calcination.

2.3. Characterization techniques

The chemical composition of the samples was measured by X-Ray fluorescence (XRF) spectrometry carried out in an X Panalytical AXIOS PW4400 with Rh tube as a source.

The instrument used for the X-ray diffraction (XRD) analysis was the X`Pert Pro PANalytical. Diffraction patterns were performed using Cu Kα radiation (40 mA, 45 kV) in a 2Θ-range of 10 to 80° and a position-sensitive detector using a step size of 0.05° and a step time of 80 s.

TEM analysis was performed in a Philips CM 200 working at 200 kV with EDS analysis and CCD camera. The average particle size, d_{av}, was estimated from equation 5 considering the relative contribution of the particles of different sizes:

$$d_{av} = \frac{\sum n_i d_i^3}{\sum n_i d_i^2} \quad (5)$$

The textural properties were analyzed by N_2 adsorption-desorption measurements at liquid nitrogen temperature. The experiments were carried out on a Micrometrics ASAP 2010 instruments. Previously the system was degassed during 2 h at 250 °C in vacuum. For the micromonolithic samples, a homemade cell that allows analyzing the complete micromonolith was used. In every case, pore size distribution was calculated using the BJH method on the desorption branch.

Temperature-programmed reduction (TPR) experiments were carried out in a conventional quartz reactor connected to a TCD detector. The reactive gas stream (5% H_2 in Ar) was flowed at 50 mL/min over 50 mg of sample, and the temperature raised at 10 °C/min from room temperature to 300 °C A CO_2-acetone trap was used to condense the gaseous products evolved, mostly water. Quantitative analyses were done by integration of the reduction signal and comparison with hydrogen consumption of a CuO reference sample.

Before the cross sections analysis, the micromonoliths were cut, embedded in a polymeric resin matrix and polished. The line analysis and the mapping micrographs were obtained in a Hitachi S4800 SEM-FEG high-resolution microscope (1–3 nm) coupled to EDX Bruker X Flash Detector 4010 (133 eV resolution).

The adherence of the catalytic layer to the substrate was evaluated using an ultrasonic method previously described [33–34]. It consists in the measurement of the weight loss caused by the exposition of the sample to ultrasound. The micromonoliths immersed in acetone were submitted to an ultrasonic treatment in a Cole Parmer ultrasonic bath (47 kHz and 130 W) for 60 min at room temperature. After that, the samples were dried, calcined and the weight loss determined by the difference in the mass of the coating before and after the ultrasonic test. The adherence is defined as the quantity of catalysts retained on the micromonolith expressed in percentage.

The isoelectric point (IEP) of the powder catalyst before slurry preparation was determined in a ZETAMASTER equipment.

Roughness of the micromonolith after thermal treatment was measured with a Mitutoyo SJ-201 P surface roughness tester.

2.4. Catalytic activity

Selective CO methanation (S-MET) measurements were carried out in a Microactivity PID Eng&Tech equipment using a 9 mm internal diameter tubular AISI316 stainless steel reactor (Autoclave Engineers). The powder samples (140 mg sieved in the 100–200 μm range), were diluted in a volume of glass particles sieved in the same diameter range (100–200 μm) equal to that occupied by the micromonolithic devices (6 cm^3). The feed gas simulating an output stream from PROX unit consists of 0.03% CO, 15% CO_2, 50% H_2, 15% H_2O and N_2 as balance. The WHSV (Weight Hourly Space Velocity) was fixed at 80,000 $ml.g^{-1} min^{-1}$. For micromonoliths a tubular reactor (16 mm inner diameter) was employed and the total flows for methanation reaction were adjusted to achieve the same WHSV as for the powder tests. Before reaction the samples were *in-situ* pre-activated at 300 °C for 2 h in.60 ml/min pure H_2 flow, purged with N_2, and then conditioned at 105 °C for 1 h within the reaction mixture. The methanation activity was evaluated from 105 °C to 270 °C. After water removal at the reactor exit, the reactant and products were analyzed by on-line gas chromatography (GC) using a Varian micro GC 4900 instrument with two channels, one with a Porapaq-Q and the other with a Molecular Sieve 5 A column, and thermal conductivity detectors (TCD). The CO_2 was analyzed by a Vaisala detector CARBOCAP GMT220. CO and CO_2 conversions (X_{CO}, X_{CO2}), and selectivity to CO methanation ($S_{CO/CO2}$) was defined as Eq. (6–8):

$$X_{CO}\,(\%) = \frac{(F_{COin} - F_{COout})}{F_{COin}} * 100 \quad (6)$$

$$X_{CO_2}(\%) = \frac{(F_{CO_2\,in} - F_{CO_2\,out})}{F_{CO_2\,in}} * 100 \quad (7)$$

$$S\frac{CO}{CO_2}(\%) = \left(\frac{X_{CO} * F_{COin}}{F_{CH_4\,out}}\right) * 100 \quad (8)$$

Being F_{CO}, F_{CO_2} and F_{CH_4} the flows in ml/min of CO, CO_2 and methane respectively, the subscripts *in* or *out* correspond to the inlet or the outlet flow.

In all cases, the methane selectivity, defined as Eq. 9, was always higher than 99.98% and only traces of ethane and ethene were detected.

$$S_{tw\,CH_4}(\%) = \left(\frac{C_{CH_4,out}/\upsilon_{CH_4}}{\sum_i C_{i,out}/\upsilon_i}\right) * 100 \quad (9)$$

$C_{i,out}$ is the product i concentration in the outlet and ν_i is the carbon numbers according to its chemical formula.

3. Results and discussion

3.1. Characterization

XRF measurements reveal that the real Ru content of the initial powder catalyst was 8.64 wt.%. This value decreases to 8.10 wt.% in the S-RuAl sample due to the additional amount of alumina incorporated to the formulation because of using Nyacol colloidal alumina as binder.

X-ray diffraction of both calcined samples RuAl and S-RuAl (Fig. 2A) confirms that the crystalline structure of the bare catalyst remains unchanged after the preparation of the slurry, being composed by RuO_2 (JCPDS 40-1290) and γ-Al_2O_3 (JCPDS 46-1215). From the broadening of the reflection peak of the (110) plane at 28° 2θ, and applying the

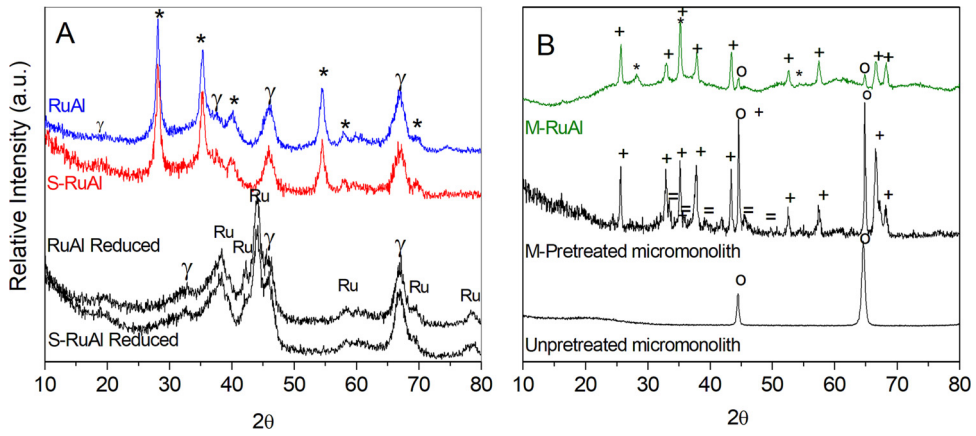

Fig. 2. XRD patterns for (A) RuAl and S-RuAl (calcined and reduced) and (B) micromonolithic devices (bare, pretreated M and coated M-RuAl). (*) RuO_2; (γ) γ-alumina; (Ru) metallic Ru; (o) martensite steel; (+) α-Al_2O_3; (=) aluminium yttrium oxide.

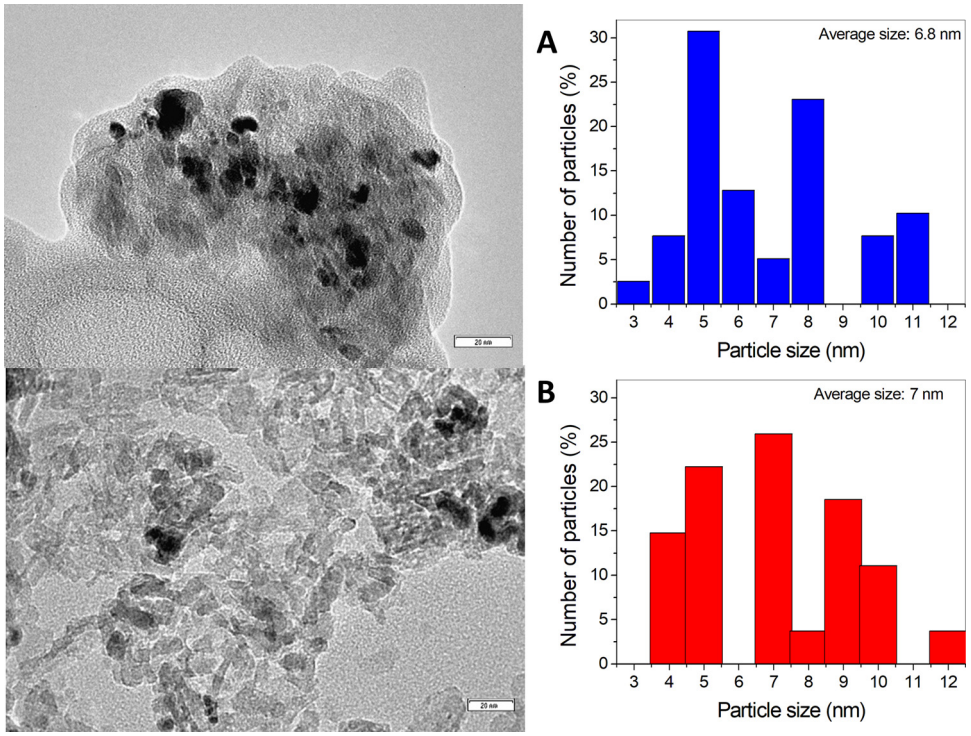

Fig. 3. TEM micrographs for reduced powder samples (A) RuAl and (B) S-RuAl.

Scherrer equation, the crystalline domain size of RuO_2 crystallites were calculated to be 11 and 10 nm for RuAl and S-RuAl, respectively. After the reduction procedure needed to activate the catalysts (300 °C, 2 h in H_2), RuO_2 is fully reduced to metallic Ru (JCPDS 06-0663, Fig. 2A) and the estimated crystallite size of Ru from the (101) plane at 44.01 ° 2θ resulted to be 7.2 and 6.5 nm RuAl and S-RuAl respectively. Although small, the changes in the average crystalline domain are significative. They imply that the slurry preparation drives to an alteration of the size of supported ruthenium. The previous milling of the powder catalyst and the concurrence of the presence of the additive PVA (with reductant character), an aqueous and acidic media, the stirring and the final thermal treatment (drying and calcination) could result in dissolution-reprecipitation or any other processes of modification of the ruthenium species. Those change the average and distribution of sizes of the metallic particles of S-RuAl from the original powder RuAl. These assumptions are confirmed by TEM analyses (Fig. 3). In this case representative TEM micrographs of the reduced powder samples as well as the ruthenium particle size distribution histograms are shown. RuAl sample presents an average Ru size of 6.8 nm, while that of S-RuAl results to be 7 nm. The values are very similar to those calculated from XRD, although the mean size determined by TEM for S-RuAl is higher than that of RuAl, the opposite trend that XRD one. This must be related with the differences in the particle evaluation method in each technique. However, despite the higher calculated average size, S-RuAl sample has a higher proportion of smaller metallic particles (lower than 4 nm).

Fig. 2B shows the XRD results for the structured catalyst (M-RuAl). For comparative purposes, those of bare and pretreated metallic substrate before catalyst deposition are also shown. Un-treated Fecralloy micromonolith shows the characteristic peaks of the martensitic structure (JCPDS 34-0396). After thermal pre-treatment, diffractions due to corundum α-Al_2O_3 (JCPDS 34-0306) and $YAlO_3$ (JCPDS 10-0425) phases appear. This thermal treatment generated α-alumina layer that is the responsible of the increment of the surface roughness (from 0.9 μm to 2.7 μm), which helps the physical anchoring of the catalyst. Obviously, its chemical compatibility with the RuAl catalyst also favors

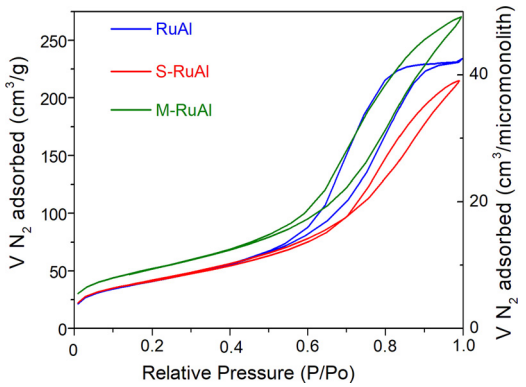

Fig. 4. N_2 adsorption–desorption isotherms obtained for RuAl, S-RuAl and M-RuAl.

Table 1
Textural properties of studied samples.

Code	SBET ($m^2\ g^{-1}$)	Pore volume ($cm^3\ g^{-1}$)	Pore size (nm)
RuAl	149	0.36	6.0
S-RuAl	153	0.38	7.5
M-RuAl	154*	0.37	7.0
Al_2O_3 Nyacol**	192	0.37	7.8

* Calculated from the amount of catalysts deposited.
** Nyacol AL20 dried and calcined at 400 °C 2 h.

the deposition. Previous studies have demonstrated that this oxide layer is formed by randomly oriented alumina whiskers with a thickness of about ≈ 3 μm and is generally accepted to be an excellent substrate to adhere catalysts [33,35].

The diffraction pattern of the micromonolithic catalysts (Fig. 2B) confirms the successful deposition of the catalyst, showing the characteristic peaks of the S-RuAl sample simultaneously with those of the pretreated metallic substrate. After reduction treatment, the RuO_2 is also reduced to metallic ruthenium (not shown). The estimated crystalline domain size of RuO_2 and Ru were 10.5 nm and 7.0 nm, respectively, intermediate values between those obtained for RuAl and S-RuAl powder catalysts. Again, the small differences points to a different degree of modification of ruthenium sizes because of the influence of the metallic substrate in the washcoating procedure and from the slurry preparation.

The N_2 adsorption–desorption isotherms of the powders and micromonolith catalysts are shown in (Fig. 4). Table 1 summarizes the textural properties of the samples. All of them show similar isotherms characteristics of mesoporous materials (type IV with H2 hysteresis loop) with complex and heterogeneous size structures having average pore radius of 6.0, 7.5 and 7.0 nm for RuAl, S-RuAl and M-RuAl respectively. A small increment in the textural properties of the S-RuAl and M-RuAl catalysts with respect to those of the parent RuAl was noticed, which is assigned to the presence of the additional alumina Nyacol. In fact, the increment matches the theoretical one calculated assuming the additional amount of alumina added (6.28 wt.%) and its textural properties (see Table 1).

The homogeneity of the S-RuAl coating onto the metallic substrate was confirmed by SEM observations (Fig. 5), where crack and spalling phenomena are not visible. The adherence of the catalyst was excellent. In this case 96 wt.% of the layer was preserved after adherence test. The mapping and in-line cross section in-depth compositional EDX analyses (Figs. 6 and 7) confirm the presence of the α-alumina layer below the RuAl coating. The RuAl layer penetrates deep in the α-alumina layer reaching the oxide–alloy interface. Thereby, EDX analysis confirms that deposited RuAl is not confined at the more external surface, penetrating through the oxide scale of the substrate. Similar results have been described for CeO_2 and Au/CeO_2 catalysts deposited on fecralloy micromonoliths [33]. This observation impedes the correct evaluation of the coating thickness from the direct measurement of the cross section SEM micrographs. Despite this, an estimative value in the 4-to-7 μm range could be obtained. A second approach to calculate the average catalytic thickness is taking into account the estimated volume of the layer [35]. This can be estimated from the amount of coating (138.3 or 147.3 mg in our case), the total surface of the metal sheet (540 cm^2), the density of the coating calculated from the pore volume (M-RuAl, 0.37 cm^3/g) and

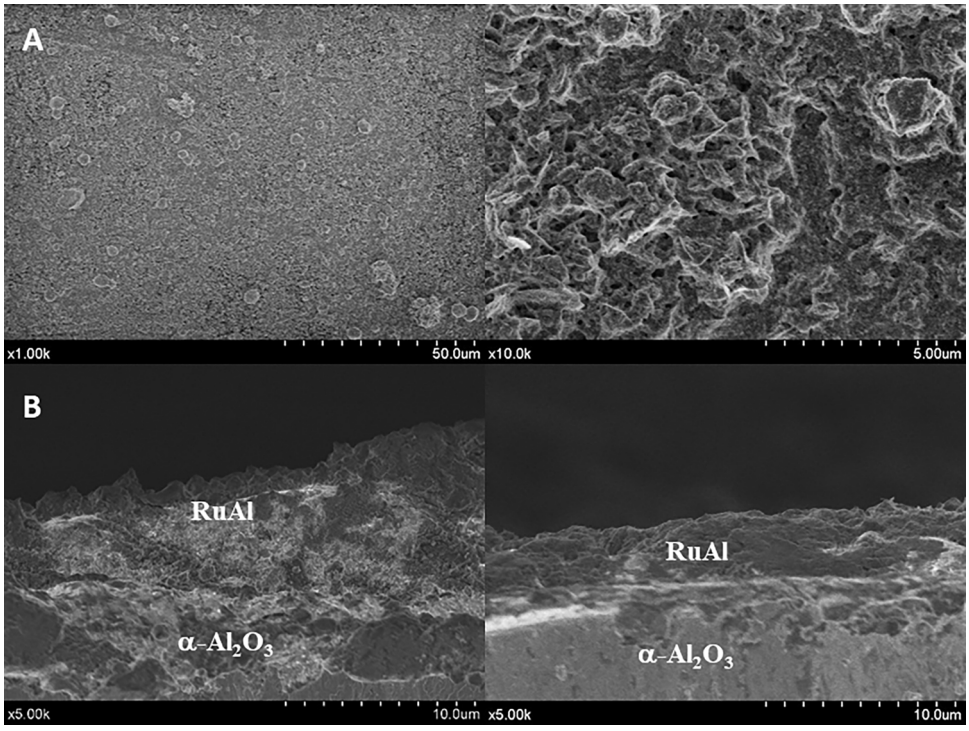

Fig. 5. SEM micrographs of M-RuAl sample; (A) top and (B) cross section views.

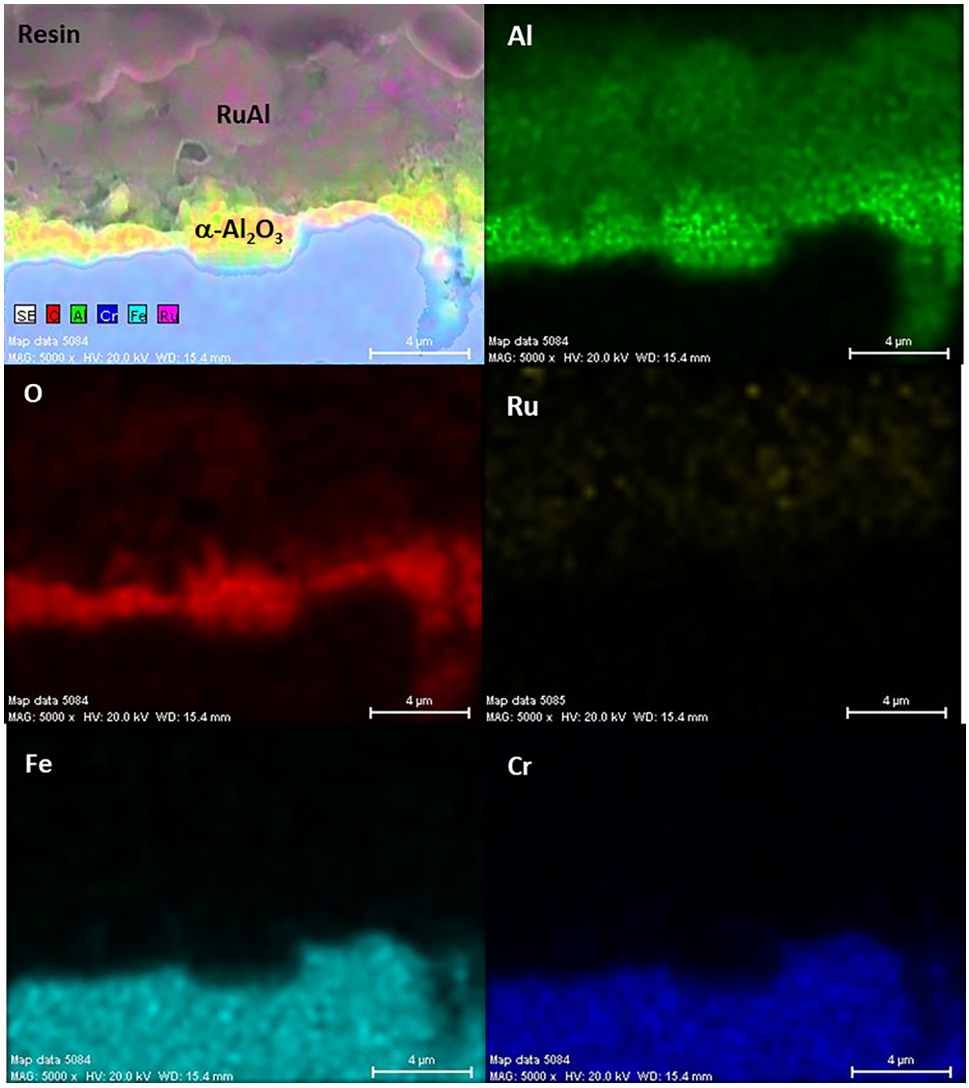

Fig. 6. Mapping of cross section of M-RuAl.

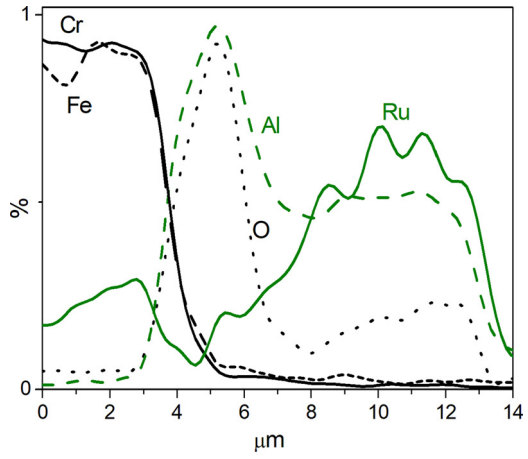

Fig. 7. In-line cross section in-depth compositional EDX analyses for M-RuAl from Fig. 6.

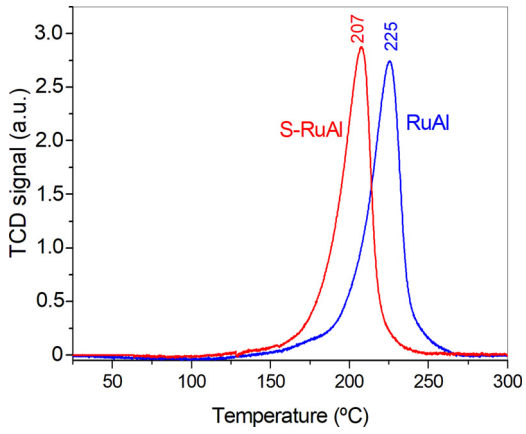

Fig. 8. TPR profile for RuAl and S-RuAl.

the apparent density of the deposited solid (4.3 g/cm^3). The average thickness obtained was ≅ 1.6 µm, a bit far of that calculated from SEM. Probably, an intermediate value is the more representative one of the average thickness of the coating. In any case, the catalytic layer thickness of the micromonoliths is small and we can discard, in principle, any mass transfer limitations produced during reaction [35–36].

Finally, no Fe and Cr diffusion from the stainless steel substrate to the catalytic layer was detected by EDX, even in the reacted micromomoliths, only the migration of aluminium oxide to the catalytic layer could be considered. In some cases, and specially under demanding

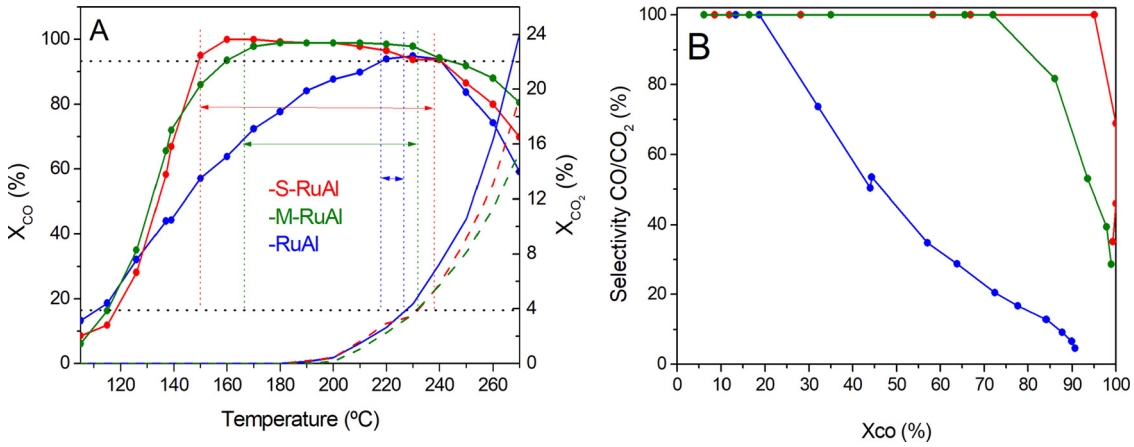

Fig. 9. (A) CO (solid lines) and CO_2 (dash lines) conversions during S-MET with powders and micromonolithic catalysts. The selective temperature range, where less than 20 ppm CO is emitted with a total H_2 consumption lower than 4% is also shown. (B) Selectivity towards CO methanation vs CO conversions. Feed composition: 0.03%CO, 15% CO_2, 50%H_2 (balance N_2); WHSV: 80,000 ml $g^{-1}.min^{-1}$.

reaction conditions, the migration of chromium and other metal cations from the fecralloy substrate to the catalytic coating have been reported in micromonolithic catalysts [33,34], resulting in a modification of the composition and catalytic performances of the bare catalyst.

The TPR profiles of the RuAl and S-RuAl are presented in Fig. 8. In both cases a single peak of H_2 consumption is observed, directly ascribed to the RuO_2 reduction to Ru°. However, the temperature at which the reduction process proceed is lower for S-RuAl than for RuAl (207 vs 225 °C). According to the literature, the reduction of RuO_2/Al_2O_3 occurs at temperatures in the 100-230 °C range, and varied with the RuO_2 crystallite size, in such a way that higher the size, higher the reduction temperature [37–40]. According to these there are two reduction peaks normally described in the literature one at ≈190 °C ascribed to well-dispersed ruthenium oxide phase, and the other at ≈223 °C, due to bulk RuO_2 reduction. Thus, the observed decrease in the reduction temperature of the RuO_2 in the slurry compared to the initial powder catalyst agrees with the lower crystallite size of RuO_2 determined from XRD, and reinforces the idea of the existence of changes in the ruthenium particle size of the catalysts during the washcoating procedure.

3.2. Catalytic activity

Fig. 9A shows the CO (X_{CO}) and CO_2 (X_{CO2}) conversions as function of reaction temperature. At the lowest temperature studied (105 °C) all catalytic systems have a certain CO methanation activity, being X_{CO} of around 10%. Increasing the temperature drives to an increment in the X_{CO} until arriving a maximum in the 160–220 °C temperature range. Further increase of temperature results in a drastic decrease of X_{CO} due to the concurrence of the reverse Water Gas Shift reaction Eq. (10), thermodynamically and kinetically favored at high temperatures [18].

$$CO_2 + H_2 \leftrightarrow CO + H_2O;\ \Delta H^\circ = +41.2\ kJ/mol \quad (10)$$

Powder RuAl catalyst does not achieve total CO conversion, a maximum X_{CO} of 94% was obtained at around 220 °C. The slurried catalyst (S-RuAl) is able to completely abate the CO molecules of the reactive stream (X_{CO} = 100%) at a lower temperature (160 °C). These catalytic activities are comparable to those reported previously for Ru/Al_2O_3 systems [41]. The structured catalysts present a catalytic behavior similar to that of the S-RuAl powder, although showing the appearance of the consequences of the R-WGS reaction (decay of the X_{CO}) at a bit higher temperatures.

For all solids, CO_2 methanation is practically zero at temperatures up to ca. 180 °C. Then, it progressively increases with the temperature (Fig. 9A). The CO_2 conversion starts when, at least, a 70% of CO is methanated. This behavior reflects that CO interacts more strongly with the catalyst surface at low temperatures, compared to CO_2. The selectivity of the CO methanation is shown in Fig. 9B. It is clear that S-RuAl presents the best selectivity. Powder RuAl sample is the less selective, meanwhile the micromonolithic systems present an intermediate behavior, although more similar to that of S-RuAl. This selectivity can be also evaluated considering the temperature range in which the CO concentration in the outstream is less than 20 ppm (more than 93.3% of CO conversion) and the total consumption of H_2 is under 4% (implying a CO_2 conversion lower than 3.2%), see Fig. 9A. This optimal range of working temperatures is 149–239 °C for S-RuAl, 165–232 °C for the micromonoliths and 217–226 °C for the powder RuAl.

The changes in the activity and selectivity of the CO methanation reaction observed among the considered catalysts can be related with the observed changes in the ruthenium dispersion and reducibility, as evidenced by TPR, XRD and TEM results. In this sense, it is reported that lower ruthenium particle sizes favor the selective CO methanation [42]. Both, the CO conversion and the selective operating temperature range, increases with the lower ruthenium particle size of the system. As proposed above, the modification of the ruthenium dispersion is probably produced during the washcoating process, caused by the presence of additives (PVA and colloidal alumina), the acidic aqueous media and the subsequent additional thermal treatment. All of this can drive to a surface structural reorganization of the metal, which, together with the presence of additional hydroxyl groups coming from the colloidal alumina added, results in a more active and selective catalysts than the parent powder. A *detailed in-situ/in-operando* FTIR study is currently under realization in order to gain insights in the mechanistic aspects of our results. The presence of the metallic substrate also alter the final ruthenium dispersion, the structured systems presenting intermediates values of activity between those of the S-RuAl and the raw RuAl. From here, in our case the structuration of the RuAl powder sample on stainless steel micromonoliths not only is possible but also drives to more active and selective systems.

4. Conclusions

The results of the present study show that the deposition of RuO_2/Al_2O_3 powder catalysts on stainless steel micromonoliths is possible. Active and selective systems for CO methanation using a flow simulating CO_2-rich reformate gases from WGS and PROX units (H_2 excess, CO_2 presence and 300 ppm CO concentration) were obtained. The slurried RuO_2/Al_2O_3 was active and selective for CO methanation as well. The changes in the activity and selectivity observed have been

related to the observed changes in the ruthenium dispersion and its reducibility as was confirmed by TPR, XRD and TEM characterization.

The metallic substrate in the washcoating procedure and the slurry preparation affected the ruthenium particle size. Thereby, the presence of PVA and colloidal alumina, the acidic aqueous media and the thermal treatment favored the surface structural reorganization of the metal towards more active catalysts. This was confirmed when the optimal range of working temperatures in which the CO concentration in the outstream is less than 20 ppm (more than 93.3% of CO conversion) and the total consumption of H_2 is under 4% (implying a CO_2 conversion lower than 3.2%) was compared. Thus, it was shifted to lower temperatures when S-RuAl and M-RuAl were used. In those cases the optimal ranges of working temperatures were from 149 °C to 239 °C for S-RuAl and from 165 °C to 232 °C for the micromonoliths, whilst it was from 217 °C to 226 °C for the RuAl powder. Further increase in temperature resulted in a drastic decrease of CO conversion due to the concurrence of the reverse Water Gas Shift reaction, thermodynamically and kinetically favored at higher temperatures.

Acknowledgments

Financial support for this work has been obtained from the Spanish Ministry of Economy and Competitiveness (ENE2012- 37431-C03-03) co-financed by FEDER funds from the European Union and from Junta de Andalucía (TEP-8196).

References

[1] C. Song, Catal. Today 77 (2002) 17–49.
[2] M. González-Castaño, T.R. Reina, S. Ivanova, M.A. Centeno, J.A. Odriozola, J. Catal. 314 (2014) 1–9.
[3] T.R. Reina, W. Xu, S. Ivanova, M.A. Centeno, J. Hanson, J.A. Rodriguez, J.A. Odriozola, Catal. Today 205 (2013) 41–48.
[4] M. Tao, Z. Xin, X. Meng, Z. Bian, Y. Lv, Fuel 188 (2017) 267–276.
[5] X. Su, J. Xu, B. Liang, H. Duan, B. Hou, Y. Huang, J. Energy Chem. 25 (2016) 553–565.
[6] S. Ronsch, J. Scheneider, S. Matthischke, M. Schluter, M. Gotz, J. Lefebre, P. Prabhakaran, S. Bajohr, Fuel 166 (2016) 273–296.
[7] A.V. Puga, Top. Catal. 59 (2016) 1268–1278.
[8] S.L. Douvartzides, F.A. Coutelieris, P.E. Tsiakaras, J. Power Sour. 114 (2003) 203–212.
[9] O. Gorke, P. Pfeifer, K. Schubert, Catal. Today 110 (2005) 132–139.
[10] M.B.I. Choudhury, S. Ahmed, M.A. Shalabi, T. Inui, Appl. Catal. A 314 (2006) 47–53.
[11] C.D. Weatherbee, C.H. Bartholomew, J. Catal. 77 (1982) 460–472.
[12] S. Abate, C. Mabrahtu, E. Giglio, F. Deorsola, S. Bensaid, S. Perathoner, R. Pirone, G. Centi, Int. Eng. Chem. Res. 55 (2016) 4451–4460.
[13] S. Abate, K. Barbera, E. Giglio, F. Deorsola, S. Bensaid, S. Perathoner, R. Pirone, G. Centi, Ind. Eng. Chem. Res. 55 (2016) 8299–8308.
[14] D. Wierzbicki, R. Debek, M. Motak, T. Grzybek, M.E. Galvez, P. Da Costa, Catal. Commun. 83 (2016) 5–8.
[15] A. Aljishi, G. Veilleux, J.A. Hernandez Lalinde, J. Kopyscinski, Appl. Catal. A 549 (2018) 263–272.
[16] F. Solymosi, A. Erdo, M. Kocsis, J. Chem. Soc. Faraday Trans. 77 (1981) 1003–1012.
[17] T. Utaka, T. Takeguchi, R. Kikunchi, K. Eguchi, Appl. Catal. A 246 (2003) 117–124.
[18] P. Panagiotopoulou, D.I. Kondarides, X.E. Verykios, Appl. Catal. B 88 (2009) 470–478.
[19] P. Panagiotopoulou, D.I. Kondarides, X.E. Verykios, Appl. Catal. A 344 (2008) 45–54.
[20] C. Garbarino, D. Bellotti, P. Riani, L. Magistri, G. Busca, Int. J. Hydrog. Energy 40 (2015) 9171–9182.
[21] C. Janke, M.S. Duyar, M. Hoskins, R. Farrauto, Appl. Catal. B 152–153 (2014) 184–191.
[22] A. Karelovic, P. Ruiz, J. Catal. 301 (2013) 141–153.
[23] T. Inui, M. Funabiki, M. Suehiro, T. Sezume, J. Chem. Soc. Faraday Trans. 1 (75) (1979) 787–802.
[24] C.D. Weatherbee, C.H. Bartholomew, J. Catal. 87 (1984) 352–362.
[25] K. Yaccato, R. Carhart, A. Hagemeyer, A. Lesik, P. Strasser, A.F. Volpe, H. Turner, H. Weinberg, R.K. Graselli, C. Brooks, Appl. Catal. A 296 (2005) 30–48.
[26] J.N. Park, E.W. McFarland, J. Catal. 266 (2009) 92–97.
[27] H.Y. Kim, H.M. Lee, J.N. Park, J. Phys. Chem. C 114 (2010) 7128–7131.
[28] R.A. Dagle, Y. Wang, G.G. Xia, J.J. Strohm, J. Holladay, D.R. Palo, Appl. Catal. A 326 (2007) 213–218.
[29] M.A. Vannice, J. Catal. 37 (1975) 449–461.
[30] K. Kowalczyk, K. Stolecki, W. Rarog-Pilecka, E. Wilckkowska, Z. Karpinski, Appl. Catal. A 342 (1–2) (2008) 35–39.
[31] L.M. Martínez T, M.I. Domínguez, O. Sanz, M.A. Centeno, J.A. Odriozola, Gold Bull. 46 (2013) 221–231.
[32] L.M. Martínez T, F. Romero-Sarria, W.Y. Hernández, M.A. Centeno, J.A. Odriozola, Appl. Catal. A 423–424 (2012) 137–145.
[33] M.I. Domínguez, A. Pérez, M.A. Odriozola, J.A. Odriozola, Appl. Catal. A 478 (2014) 45–57.
[34] L.M. Martínez T, M.I. Domínguez, N. Sanabria, W.Y. Hernández, S. Moreno, R. Molina, J.A. Odriozola, M.A. Centeno, Appl. Catal. A 364 (2009) 166–173.
[35] O.H. Laguna, M. González Castaño, M.A. Centeno, J.A. Odriozola, Chem. Eng. J. 275 (2015) 45–52.
[36] D.I. Potemkin, P.V. Snytnikov, V.D. Belyaev, V.A. Sobyanin, Chem. Eng. J. 176–177 (2011) 165–171.
[37] Y. Zhao, J. Zhou, J. Zhang, S. Wang, Catal. Lett. 131 (2009) 597–605.
[38] Z. Mei, Y. Li, M. Fan, M.D. Argyle, J. Tang, Int. J. Hydrog. Energy 39 (2014) 14808–14816.
[39] P.S. Sankar Reddy, N. Pasha, M.G.V. Chalapathi Rao, N. Lingaiah, I. Suryanarayana, P.S. Sai Prasad, Catal. Commun. 8 (2007) 1406–1410.
[40] P. Betancourt, A. Rives, R. Hubaut, C.E. Scott, J. Goldwasser, Appl. Catal. A 170 (1998) 307–314.
[41] P. Djinović, X. Galleti, S. Specchia, V. Specchia, Top. Catal. 54 (2011) 1042–1053.
[42] S. Tada, R. Kikuchi, K. Urasaki, S. Sagokawa, Appl. Catal. A 404 (2011) 149–154.